$t = 0.5$ indicated by the dashed curve, is shown for comparison. Inside the initial jet, $\omega_A = 1$ and outside of the jet $\omega_A = 0$. Figure 2 shows how the diffusion toward the wall is greater. This is caused by the velocity profile of the boundary layer. For $t = 0.7$ the maximum concentration has dropped to 0.4 and the location of the maximum contour has drifted toward the wall. Two of the smaller concentration lines end on the wall surface.

When $t = 1.64$, as shown in Fig. 3, the maximum concentration drops to 0.145 and the contour line has moved closer to the wall. Near the wall where the velocities are small, a fluid element has more time to diffuse as it moves between the stations given in Figs. 2 and 3. As a result, there is a greater lateral movement of the concentration lines in the vicinity of the wall.

The contour shapes shown here are similar to those measured in the supersonic mixing experiments described in Refs. 1–3. However, in high-speed flows, the compressibility and vorticity diffusion effects which were neglected in the present analysis may be important. In those cases where these effects are small, the present method may yield useful results.

References

[1] Henry, J. R., "Recent Research on Fuel Injection and Mixing and Piloted-Ignition for Scramjet Combustors," *Twelfth Symposium on Combustion*, The Combustion Inst., Pittsburgh, 1969, pp. 1175–1182.

[2] Torrence, M. G., "Concentration Measurements of an Injected Gas in a Supersonic Stream," TN D-3860, April 1967, NASA.

[3] Rogers, R. C., "The Penetration and Mixing of a Sonic Hydrogen Jet Injected Normal to a Mach 4 Airstream," M.S. thesis, March 1970, Virginia Polytechnic Inst., Blacksburg, Va.

[4] Bird, R. B., Stewart, W. E., and Lightfoot, E. N., *Transport Phenomena*, John Wiley & Sons, New York, 1960, p. 557.

[5] Baker, A. J., "A Numerical Solution Technique for a Class of Problems in Fluid Dynamics, Formulated with the Use of Discrete Elements," TCTN-1005, 1969, Bell Aerosystems, Buffalo, N.Y.

[6] Baker, A. J., "Numerical Solution to the Dynamics of Viscous Fluid Flow by a Finite-Element Algorithm; A First Step Towards Computational Continuum Mechanics," *Proceedings of the International Association for Shell Structures Pacific Symposium*. Univ. of Hawaii, Oct. 1971.

[7] Baker, A. J., "A Finite-Element Computational Theory for the Mechanics and Thermodynamics of a Viscous, Compressible, Multi-Specie Fluid," Rept. 9500–920200, 1971, Bell Aerospace, Buffalo, N.Y.

[8] Finlayson, B. A. and Scriven, L. E., "The Method of Weighted Residuals—A Review," *Applied Mechanics Review*, Vol. 19, No. 9, 1966, pp. 735–748.

[9] Nigro, B. J., "The Derivation of Optimally Stable, K-Stage, One-Step, Explicit Numerical Integration Methods," TCTN-1008, 1970, Bell Aerospace, Buffalo, N.Y.

Pressure Distribution on a Yawed Wedge Interacted by an Oblique Shock

M. G. CHOPRA*

Defence Science Laboratory, Delhi, India

AN analytical method developed by Lighthill[1,2] for plane normal shock and later extended for oblique shocks by Srivastava[3] and Srivastava and Chopra[4] has now been applied to the diffraction of oblique shocks advancing over yawed wedges for the case when the relative flow behind the reflected shock is subsonic. Computations have also been undertaken to explore the pressure distribution on the wedge surface.

Received December 14, 1971; revision received February 1, 1972. The author is thankful to M. J. Lighthill, and R. R. Aggarwal for their interest in the work; R. S. Srivastava for his guidance, and Director Defence Science Laboratory for allowing its publication.

Index categories: Shock Waves and Detonations; Supersonic and Hypersonic Flow; Nonsteady Aerodynamics.

* Senior Scientific Officer.

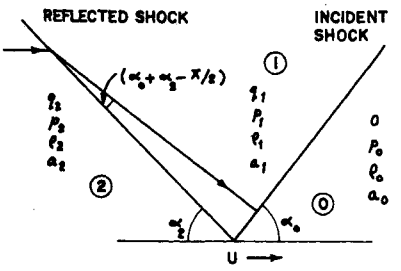

Fig. 1 Oblique shock configuration.

As the oblique shock configuration (Fig. 1) advances over a yawed wedge (shock line making some nonzero angle with the leading edge of the wedge), the point of intersection of the leading edge and the shock line moves with the velocity $U \csc \chi$, U and χ being the velocity of the shock line and angle of yaw, respectively. The whole configuration can be brought to rest by superimposing a velocity $U \csc \chi$ along the leading edge (Fig. 2) and for ensuring conical flowfield behind the reflected shock the angle of yaw must satisfy the inequality

$$\sin^2 \chi < U^2/(a_2^2 + 2Uq_2 - q_2^2)$$

In fact, the limit on χ depends both on the incident shock strength and the angle of incidence. For a particular shock strength as the angle of incidence increases from the sonic angle to the extreme angle the limiting value of χ decreases and attains its minimum for extreme angle. The limit on χ for different shock strengths taking angle of incidence equal to extreme angle is depicted graphically (Fig. 3) and it is observed that it decreases slowly as the shock strength varies from 0 to 0.6, increases slowly thereafter and finally shows steep rise as the shock strength varies from 0.9 to 1.0. Chester[5] also found out a similar restriction on the angle of yaw but it varied with shock strength only.

Let the perturbations introduced in the flow behind the reflected shock have components u_1, v_1 and w_1 referred to Cartesian coordinate system (x', y', z') such that z' axis is along the axis of the cone of disturbance and x' is perpendicular to z' axis lying in the plane of the wedge and passing through the point of intersection of shock line and leading edge. The flow picture (Fig. 4) obtained in a plane normal to the axis of the Mach cone is the same as for the case of interaction of oblique shock with unyawed wedges (shock line making zero angle with the leading edge) with the only difference that in the problem of interaction of unyawed wedges the flow picture grows with respect to time whereas in the present case it can be regarded to be growing with the axis of the cone of disturbance. In fact, for the unyawed case the cone of disturbance will degenerate into a cylinder, the axis of the cone becoming parallel to the leading edge and the vertex of the cone approaching infinity. With the help of conical field transformations used by Chester,[5] the physical situation may be translated into the following boundary value problem in terms of perturbed pressure p. Differential equation

$$\frac{\partial^2 p}{\partial x^2} + \frac{\partial^2 p}{\partial y^2} = \left(x\frac{\partial}{\partial x} + y\frac{\partial}{\partial y} + 1\right)\left(x\frac{\partial p}{\partial x} + y\frac{\partial p}{\partial y}\right) \qquad (1$$

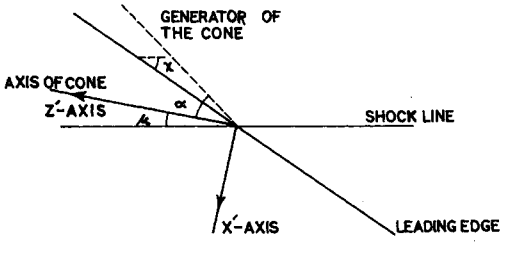

Fig. 2 Configuration after interaction in the x'–z' plane.

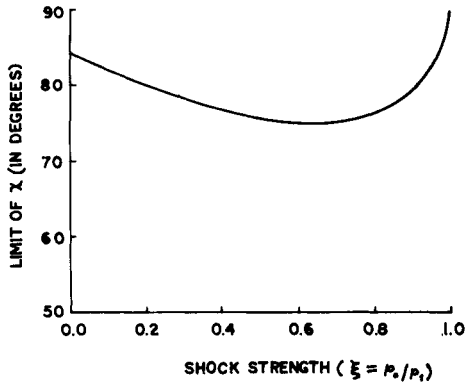

Fig. 3 Limit on the angle of yaw for different incident shock strengths.

Boundary conditions: on the wedge surface

$$\partial p/\partial y = 0 \tag{2}$$

on the Mach cone

$$p = 0 \quad \text{for} \quad x > -m^{-1} \quad \text{where} \quad m = \tan(\chi-\mu)/\tan\alpha$$
$$= -m\delta \sec\alpha \cos\chi/(m^2-1)^{1/2} \quad \text{for} \quad -m < x < -m^{-1} \tag{3}$$

α and μ being the semiangle of the cone of disturbance and the angle that the axis of the cone of disturbance makes with the reflected shock.

On the reflected-diffracted shock

$$\frac{\partial p/\partial x}{\partial p/\partial y} = \frac{y\{(k-y\cot\alpha_2\sec\mu)+(C-By)/(C_3-B_3y)\}+(k-y\cot\alpha_2\sec\mu)(C_1-B_1y)/(C_3-B_3y)}{\{1-(k-y\cot\alpha_2\sec\mu)^2\}} \tag{4}$$

where $k = \tan\mu/\tan\alpha$ and B's and C's are constants known in terms of the physical parameters defining the problem viz., incident shock strength, incident angle and angle of yaw.

Nondimensionalized perturbed velocity component at the shock wall junction is

$$v = \delta\cos\chi\sec\alpha$$

and therefore

$$\int\frac{\partial v}{\partial y}dy = \int\frac{C_1-B_1y}{C_3-B_3y}dp = \delta\cos\chi\sec\alpha \tag{5}$$

wherein the integral has been taken along the diffracted part of the shock.

It may, however, be pointed out that there is a slight error in the transformation

$$w = (V_1-w_1)/q_1\sin\alpha$$

used by Chester[5] and in fact, it should have been $w = -w_1/q_1\cdot\sin\alpha$.

Using Busemann's transformation

$$x = r\cos\theta, \quad y = r\sin\theta, \quad \rho = [1-(1-r^2)^{1/2}]/r$$

and conformal transformations

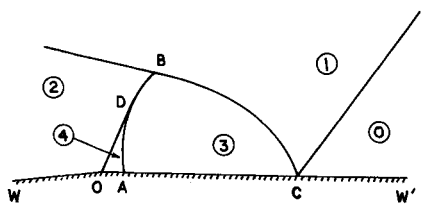

Fig. 4 Flow picture in a plane perpendicular to the axis of the cone of disturbance.

Fig. 5 Region of disturbance in z_1-plane.

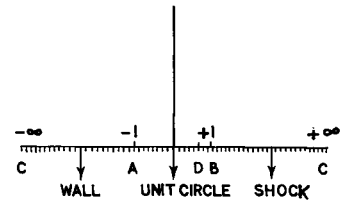

$$Z = (K+iK')\{i-2K'/[\zeta-(K+iK')]\} \tag{6}$$

and

$$z_1 = \tfrac{1}{2}\{[(aZ+1)/(aZ-1)]^{\pi/\lambda}+[(aZ+1)/(aZ-1)]^{-\pi/\lambda}\} \tag{7}$$

with $K = k\sin\phi$, $K' = (1-K^2)^{1/2}$, $\phi = \cot^{-1}(\cot\alpha_2\sec\mu)$

$$\zeta = \rho e^{i\Theta}, \qquad \Theta = \theta-\pi/2+\phi$$
$$a = (K'\sin\phi+K\cos\phi)/(K'\sin\phi-K\cos\phi),$$
$$\lambda = \cot^{-1}\{\cos\phi/(\sin^2\phi-K^2)^{1/2}\}$$

The region bounded by the curvilinear triangle is mapped on to lower half-plane (Fig. 5) and the shock boundary condition (4) becomes

$$\frac{\partial p/\partial y_1}{\partial p/\partial x_1} = \frac{K'^2G_1+(K'^2D_1-K^2G_1')\tan\Theta+(K'^2E_1-K^2D_1')\tan^2\Theta+(K'^2F_1-K^2E_1')\tan^3\Theta}{(1-K^2\sec^2\Theta)^{1/2}(G_1'+D_1'\tan\Theta+E_1'\tan^2\Theta)}$$

The wall boundary condition becomes

$$\partial p/\partial y_1 = 0 \quad \text{for} \quad y_1 = 0, x_1 < -1$$

On DB, $p = 0$ and on AD,

$$p = m\delta\cos\chi\sec\alpha/(m^2-1)^{1/2}$$

and the condition holding at D becomes

$$\int_{x_0-\varepsilon}^{x_0+\varepsilon}\frac{\partial p}{\partial x_1}dx_1 = \frac{m\delta\cos\chi\sec\alpha}{(m^2-1)^{1/2}} \tag{9}$$

the position of D being

$$x_0 = \cos(2\pi\Sigma/\lambda) \tag{10}$$

with

$$\Sigma = \tan^{-1}\left[\frac{1+m(K\sin\phi-K'\cos\phi)}{a\{(m\sin\phi+K)-K'(m^2-1)^{1/2}\}}\right]$$

Condition (5) becomes

$$\int_{+\infty}^{+1}\frac{C_1-B_1y}{C_3-B_3y}\cdot\frac{\partial p}{\partial x_1}dx_1 = \delta\cos\chi\sec\alpha \tag{11}$$

The solution of the above boundary value problem is obtained by the introduction of a complex function $w(z_1) = (\partial p/\partial x_1)-i(\partial p/\partial y_1)$ which is regular in the lower half-plane. The discontinuity condition (9) indicates that near $z_1 = x_0$

$$w(z_1) \sim \frac{-im\delta\cos\chi\sec\alpha/\pi(m^2-1)^{1/2}}{(z_1-x_0)} \tag{12}$$

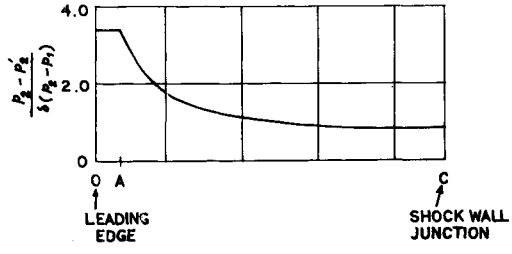

Fig. 6 Pressure distribution on the wedge surface along the section perpendicular to the axis of the cone of disturbance ($\xi = 0$, $\chi = 40°$, $\alpha_0 = 39.97°$, $\delta = 0.1$ rad).

Now that the imaginary part of $\log w(z_1)$ is known all along the real axis of z_1 plane, the extension of Poisson's integral gives

$$\log \frac{w(z_1)}{H_1} = -\frac{1}{\pi}\int_{-\infty}^{+\infty}\left[\tan^{-1}\left\{-\frac{\partial p/\partial y_1}{\partial p/\partial x_1}\right\}\Big/(t-z_1)\right]dt \quad (13)$$

where H_1 is a real constant. This completes the theoretical solution of the problem.

A brief outline for evaluating pressure on the wall and numerical discussions of the problem have been taken up for the case when the leading-edge lies outside the cone of disturbance and the results for other cases can be obtained on similar lines. For a shock of infinite strength impinging at an incidence of 39.97° with $\chi = 40°$ the shock boundary condition becomes

$$\frac{\partial p/\partial y_1}{\partial p/\partial x_1} = \frac{0.16931 - 0.09429\tan\Theta - 0.05812\tan^2\Theta + 0.02859\tan^3\Theta}{(0.75607 - 0.24393\tan^2\Theta)^{1/2}(0.36323 + 0.11275\tan\Theta - 0.06569\tan^2\Theta)} \quad (14)$$

where $\tan\Theta = 1.76055[(Z^2-1)/(Z^2+1)]$ and Z is in turn known in terms of x_1 through Eqs. (6), (7) and Busemann's transformation.

From Eq. (13), making use of Simpson's rule after removing the singularities of the integral

$$w(z_1) = \frac{G\delta[H(z_1-x_0)-1]\cos\chi\sec\alpha}{(z_1-x_0)(z_1^2-1)^{1/2}}\cdot(z_1-1)^{\beta/\pi}\cdot e^{\Phi+i\beta} \quad (15)$$

where

$$\Phi = \frac{z_1}{12\pi}\left[\frac{1.51716-\beta}{1} + \frac{4(0.00505-\beta)}{(1-0.25z_1)} + \frac{2(-0.10311-\beta)}{(1-0.50z_1)} + \frac{4(-0.22845-\beta)}{(1-0.75z_1)} + \frac{(-1.57080-\beta)}{(1-z_1)}\right]$$

and

$$\beta = \tan^{-1}\{-(\partial p/\partial y_1)/(\partial p/\partial x_1)\}$$

On the wedge surface represented by $x_1 < -1$ in z_1 plane, $w(z_1)$ is given by Eq. (15) with $\beta = 0$. From Eqs. (15) and (12)

$$G = [m/\pi(m^2-1)^{1/2}]\cdot(1-x_0^2)^{1/2}\cdot e^{-\Phi}$$

which yields, after substituting for x_0 from Eq. (10), $G = 0.75595$. The other constant H is obtained by substituting for $\partial p/\partial x_1$ from Eq. (15) in Eq. (11) and evaluating the integral by Simpson's rule after taking appropriate number of intervals. Now that $w(z_1)$ is completely known the pressure distribution on the wedge surface along a line perpendicular to the axis of the Mach cone is found by integrating $\partial p/\partial x_1$ between -1 and x_1, x_1 taking values between -1 to $-\infty$. The value of p at $x = -1$ being given by Eq. (3) its value at different x_1 can therefore be obtained. As x_1 varies from -1 to $-\infty$ the position of the point corresponding to x_1 in the physical plane varies from -1 to $+0.94113$ and the correspondence between x_1 and x is worked out backward with the help of Eqs. (7), (6) and Busemann's transformation.

In Fig. 6 the value of

$$(p_2-p_2')/\delta(p_2-p_1) = a_2\rho_2 q_2/(p_2-p_1)\cdot(-p/\delta)$$

is plotted for different points of the wedge surface. The curve maintains a constant value from the leading edge to the point of intersection of the unit circle and wedge segment and thereafter decreases up to the point of intersection of reflected-diffracted shock and the wall. It may be pointed out that the comparison with the unyawed case has not been made because here pressure deficiency is plotted along a line perpendicular to the axis of the Mach cone whereas Srivastava[3] has determined pressure distribution on a line perpendicular to the leading edge. This comparison can, however, be made for points very close to the leading edge and it is seen that yaw results in higher pressure deficiency as expected.

References

[1] Lighthill, M. J., "The Diffraction of Blast I," *Proceedings of the Royal Society*, Ser. A, Vol. 198, 1949, pp. 454–470.

[2] Lighthill, M. J., "The Diffraction of Blast II," *Proceedings of the Royal Society*, Ser. A, Vol. 200, 1950, pp. 554–565.

[3] Srivastava, R. S., "Diffraction of Blast Wave for the Oblique Case," Current Paper 1008, 1968, Aeronautical Research Council, England.

[4] Srivastava, R. S. and Chopra, M. G., "Diffraction of Blast Wave for the Oblique Case," *Journal of Fluid Mechanics*, Vol. 40, Pt. 4, 1970, pp. 821–831.

[5] Chester, W., "Diffraction and Reflection of Shocks," *Quarterly Journal of Mechanics and Applied Mathematics*, Vol. 7, 1954, pp. 57–82.

Filtering with Perfectly Correlated Measurement Noise

ROBERT REASENBERG*
MIT, Cambridge, Mass.

IN the usual implementation of the Kalman filter it is assumed that the measurement noise covariance matrix is diagonal. Although this white-noise assumption leads to considerable simplification, it is not realistic. In particular, there are data types which are formed by differencing adjacent members of a sequence of observations. Such data are highly correlated and contain more information than is indicated by the usual analysis.

A useful measure of the information contained in a set of data is the covariance of a group of parameters estimated from the set. When the variance of a single estimated parameter is taken as the information measure, a (scalar) ratio G between two such measures indicates the relative information content of the corresponding sets of data. Excessive reliance on such a ratio would certainly be naive as evidenced by the strong dependence of G on the choice of estimated parameter. However it can provide some insight into the effect of the off-diagonal terms of the noise covariance matrix on the information content of a set of data.

We shall examine (radar) Doppler data which is formed by mixing the returning microwave signal with a replica of the transmitted signal, counting the cycles of the beat, and sampling the counter at evenly spaced intervals t_i. The average Doppler frequency during an interval is the difference between the cycle counts at the ends of the interval divided by the length of the interval $\tau = t_i - t_{i-1}$.

If each counter sample n_i has an independent, zero mean, Gaussian noise v_i associated with it, then the Doppler frequency f_i has a covariance R_{ij}

$$v_i \sim N(0, Q) \quad (1a)$$

$$\langle v_i v_j \rangle = Q\delta_{ij} \quad (1b)$$

$$f_i = \frac{n_i - n_{i-1}}{\tau} \quad (2)$$

$$R_{ij} = \left\langle \frac{v_i - v_{i-1}}{\tau}\,\frac{v_j - v_{j-1}}{\tau} \right\rangle \quad (3a)$$

$$= \frac{2Q}{\tau^2}U_{ij}(\alpha)\Big|_{\alpha=-1/2} \quad (3b)$$

where

$$U_{ij}(\alpha) = \begin{cases} 1 & i = j \\ \alpha & |i-j| = 1 \\ 0 & |i-j| > 1 \end{cases} \quad (4)$$

Received December 13, 1971; revision received February 4, 1972. Work Supported under NASA Contract 952694.

Index categories: Spacecraft Tracking; Navigation, Control, and Guidance Theory.

* DSR Research Staff, Department of Earth and Planetary Sciences